Brightness and purity of a room-temperature single-photon source in the blue-green range

Francis Granger, Saransh Raj Gosain, Gilles Nogues, Edith Bellet-Amalric, Joel Cibert, David Ferrand, Kuntheak Kheng

Brightness and purity of a room-temperature single-photon source in the blue-green range

Francis Granger [1,2,*] **Saransh Raj Gosain** [1] **Gilles Nogues** [2] **Edith Bellet-Amalric** [1] **Joël Cibert** [2] **David Ferrand** [2] **Kuntheak Kheng** [1]

[1] Univ. Grenoble-Alpes, CEA, Grenoble INP, IRIG, PHELIQS, NPSC, 38000 Grenoble, France
[2] Univ. Grenoble-Alpes, CNRS, Inst. NEEL, 38042 Grenoble, France
[*] Correspondence: francis.granger@cea.fr

ABSTRACT

Single-photon sources are crucial for developing secure telecommunications. However, most systems operate at cryogenic temperatures. Here, we discuss a promising solid-state system emitting single photons at room temperature in the blue-green range, allowing for quantum communications in free space and underwater. The active element is a core-shell ZnSe tapered nanowire embedding a single CdSe quantum dot grown by molecular beam epitaxy. A patterned substrate enables a thorough study of the one and same nanowire by different methods. Our source exhibits anti-bunching with $g^2(0) < 0.3$ near peak intensity and shows high brightness. This work paves the way for developing on-chip single-photon sources operating at non-cryogenic temperatures.

Quantum communication is a rapidly growing field with enormous potential for secure data transmission. One of the significant challenges in this field is the development of single-photon sources (SPS) that can effectively generate on-demand single photons for use in quantum information systems. The main advantage of using solid-state systems such as quantum dots (QDs) is that they present high single-photon purity, making them ideal for use in quantum key distribution (QKD) protocols [1]. In QKD, single photons are used as flying qubits to transmit information, and the purity of the source is critical to ensuring the security of the transmission. In contrast to classical bits, flying qubits cannot be copied, making it impossible for eavesdroppers to intercept the transmission. Many single-photon sources are based on III-V grown QDs and exhibit spectrally narrow lines in near infra-red when operating at cryogenic temperatures, with impressive performances in terms of brightness and purity [2 3]. However, the need for cryogenic temperatures is a major drawback for practical implementation of these emitters in quantum information systems. Nitride semiconductors have shown room-temperature single-photon emission at different energies [4–6]. CdSe QDs inserted in ZnSe offer an alternative solution, as they are operational at room temperature [7]. They emit in the blue-green range, thus allowing for free-space long-distance communication in seawater and air [8]. This makes them an attractive alternative for real-world implementation of SPS in quantum information systems. Efficient extraction of the light from QDs is a critical issue towards with high emission rates. A good way to achieve this is to embed a QD in a nanowire (NW) [9 10] which acts as a waveguide channeling the photons emitted by the QD. Furthermore, a tapered NW improves control of the emission properties of the system. The taper shape adiabatically expands the guided mode and reduces the divergence angle, increasing the collection efficiency. We report here on a SPS based on a semiconductor QD-tapered NW, with purity $g^2(0) < 0.3$, emitting in the blue-green range and operating at room temperature. Our study focuses on a unique QD-NW which was submitted to a whole range of characterizations, although other emitters on the same sample exhibit similar properties.

First, we have used molecular beam epitaxy (MBE) to grow, at 350°C on a GaAs (111)B substrate, the ZnSe core embedding a CdSe QD near its top (Fig. 1(a)). This was followed by the growth at 320°C of a tapered ZnSe shell.

Growth conditions are detailed in Refs.[11] and[12]. The epiready substrate was patterned before growth, enabling the NW position to be marked and allowing several observations on the same NW by switching from one experimental setup to another.

The NW depicted in this article was selected from its far-field emission diagram recorded using Fourier imaging[13]. To this purpose, we use a high numerical aperture objective ($NA = 0.72$) along with a cw excitation laser at 405 nm. Then we performed micro-photoluminescence measurements (μ-PL) as well as time-resolved photoluminescence (TRPL) in a second setup with non-resonant pulsed excitation from a titanium-sapphire laser frequency-doubled to 440 nm (repetition time $T_0 = 13.1$ ns, frequency $f_{rep} = 76$ MHz). Light is collected through a $NA = 0.55$ objective and sent to a spectrometer equipped with a 600 grooves/mm grating (input slit width 0.2 mm). Complementary measurements done at cryogenic temperature were performed using a 1800 grooves/mm grating and a slit width of 0.05 mm. A Hanbury Brown and Twiss (HBT) setup composed of two fast avalanche photodiodes (APD) allows correlation and decay-time measurements to characterize the purity of the SPS. The last measurement was to observe the NW under a Scanning Electron Microscope (SEM).

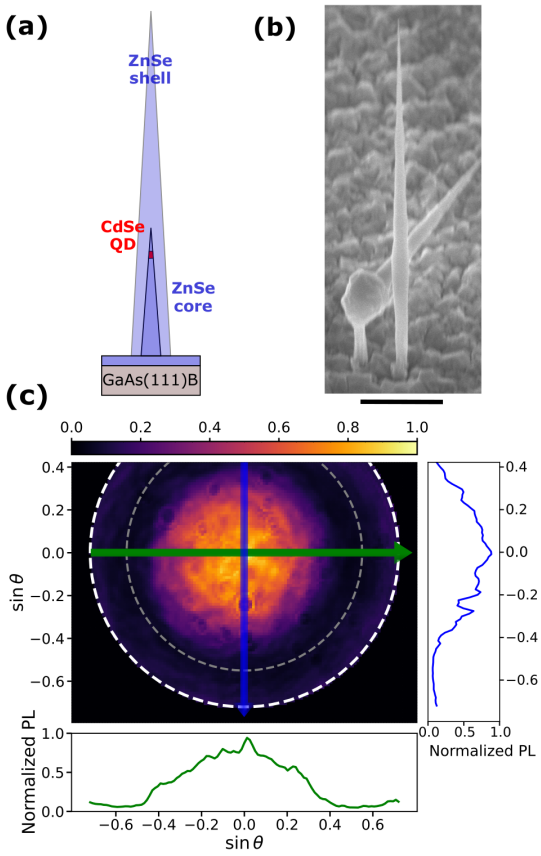

Figure 1: **(a)** Schematic of the core-shell tapered NW. **(b)** Tilted view (45°) SEM image of the studied NW (scale bar 1 μm). **(c)** Radiation pattern of the same QD-NW, under 14 μW excitation. The white dotted line represents the numerical aperture of the microscope objective ($NA = 0.72$) used for Fourier imaging, and the gray circle the numerical aperture of the microscope used for spectra and TRPL measurements ($NA = 0.55$). The cross-sections (blue and green curves) are averaged over 5 pixels, and show a Gaussian cross-section profile.

A vertical and taper-shaped NW is displayed in Fig. 1(b) alongside with another nanowire that is laid down. The 1 μm scale bar is of the same order as the diameter of the excitation laser spot. The vertical NW being studied has a base diameter of 140 nm and a height of 5 μm. The far-field diagram in Fig. 1(c) shows that the photons emitted upward

exhibit a Gaussian mode profile with divergence angle α such that $\sin\alpha = 0.3$ at half maximum, in agreement with previous studies on vertical NWs shaped with a small taper angle[9,10]. The NW shape ensures an adiabatic coupling between the guided mode and free space, leading to an observed collection efficiency close to unity within $NA = 0.72$ (thick dashed line in Fig. 1(c)) and 85% within $NA = 0.55$ (thin dashed line). We note that light emitted towards the substrate is lost, leading to a theoretical maximum source efficiency close to 50%. Additionally, the microscope objective with $NA = 0.55$ shows a transmission of 90% at the wavelength of interest[14]. Thus, an ideal SPS inserted in the present NW is limited to 0.36 photon per pulse at the output of this objective.

The QD-NW room temperature μ-PL spectra are shown in Fig. 2 for values of the pulsed excitation power P ranging from 0.2 to 6 μW. We observe two peaks at 582.5 nm (L1) and 586.5 nm (L2). It can be seen qualitatively that L1 intensity grows linearly with P, while L2 grows at a faster rate. At P =6 μW, the QD starts to saturate. Using the setup calibration explained in Supplement 1, the number of photons collected out of the microscope objective for L1 and L2 together yield to a promising value of 0.28 photon per pulse. This is discussed later in the article.

The onset of saturation around P =6 μW was confirmed by further measurements up to 20 μW. However, these measurements at high-power caused an evolution of the spectrum, as seen in the inset of Fig. 3(a) for P =5.3 μW. L1 intensity decreased significantly and L2 to a lesser extent. After this evolution, L1 + L2 signals yield to 0.09 photon per pulse, a value which was observed to be constant for weeks after this initial decrease.

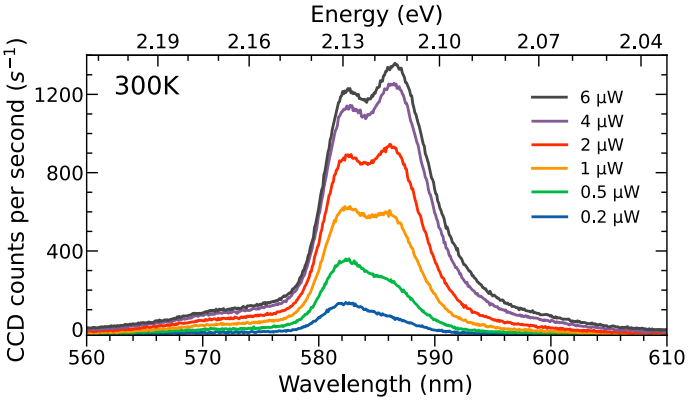

Figure 2: Power-dependent spectra of the QD-NW of Fig. 1(b).

Figure 3 shows the TRPL signal of the QD-NW emission within a spectral window of 585 ± 0.5 nm (blue arrow labeled 1 in the inset). The solid line is the convolution of the response function of the setup (a Gaussian with a FWHM of 60 ps[15]), and a sum of three exponential functions and a constant baseline

$$I(t) = \sum_{i=1}^{3} A_i \exp(-\frac{t}{\tau_i}) + B \tag{1}$$

The main component is a decay with a short lifetime $\tau_2 = 0.74$ ns. There is also a weak, slow component, $A_3 \exp(-\frac{t}{\tau_3})$ with $\tau_3 = 3$ ns and $A_3/A_2 < 0.06$. The term $A_1 \exp(-\frac{t}{\tau_1})$ with $A_1 < 0$ is introduced to describe a possible repopulation of the QD emitting state by other states. However, we obtain $\tau_1 < 30$ ps and with $|A_1|/A_2 < 0.07$, which suggests that this is not a significant effect, probably hidden by the time-resolution of the APD[15].

The purity of the SPS was determined by a HBT autocorrelation measurement. The coincidence histogram for the same conditions as in Fig. 3(a) (blue arrow) is presented in Fig. 3(b). Under pulsed excitation, a series of correlation

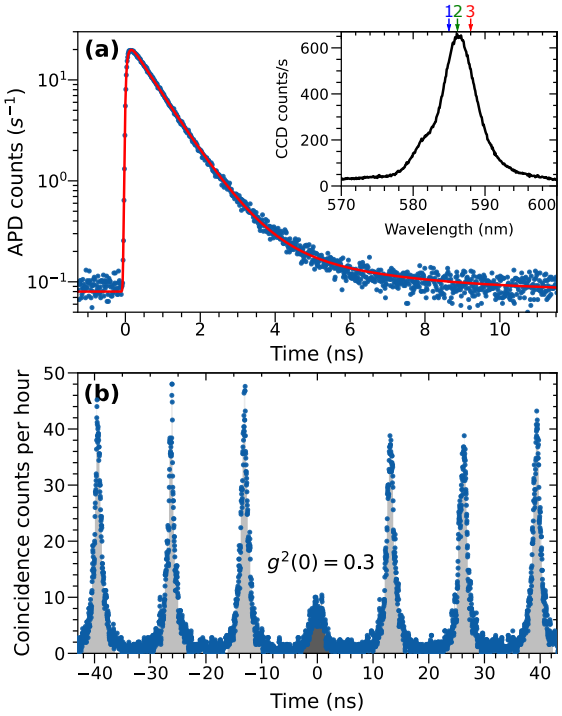

Figure 3: Room temperature TRPL measurements on the same NW as in Fig. 1(b). **(a)** TRPL decay of the QD at 585 ± 0.5 nm (P =5.3 µW). The solid red line is a fit to the data using Eq. 1. The inset displays the µ-PL spectrum at 5.3 µW, with arrows indicating the central positions of spectral bandwidths (1 nm) used for time-resolved measurements: 585 ± 0.5 nm (blue arrow 1), 586.2 ± 0.5 nm (green arrow 2), and 588 ± 0.5 nm (red arrow 3). **(b)** Second-order intensity correlation of the QD emission under 5 µW pulsed excitation. The blue symbols show the histogram of delay times between photons detected on the start-stop APDs, averaged over seven channels. The value $g^2(0) = 0.3$ has been calculated by removing a constant baseline and computing the ratio of the central peak area (dark grey) to the lateral ones (light grey).

peaks appear, with equal spacing given by the laser repetition period T_0. The peak widths are in agreement with the lifetime τ_2. As $\tau_2 \ll T_0$ in this case, the purity is computed using the ratio of the central peak area to the lateral ones. At 585.0 nm, our system exhibits a second-order correlation at zero delays $g^2(0) = 0.3$, which is below the threshold of 0.5 considered as a signature of a single-photon emission.

It is difficult to identify the nature of L1 and L2 from the spectra at room temperature, but this can be done by a comparison with the PL spectrum recorded at cryogenic temperature, shown in Fig. 4(c). Sharp zero-phonon lines lie on top of broad acoustic-phonon sidebands. Polarization-resolved PL spectra (not shown) allow us to observe a fine structure splitting with opposite signs for two of those lines, therefore attributed to the neutral exciton X and biexciton XX. This agrees with the linear and quadratic behavior observed in Fig. 2. The most intense line on Fig. 4(c) shows no fine structure. Hence, it is attributed to a charged exciton CX. A similar spectral arrangement of the X, CX, and XX lines has been observed on previous, similar samples[16]. The CX line was attributed to the positively charged exciton X^+ in Ref.[17], and the lines with energies smaller than XX were previously attributed to the charged biexciton CXX in Refs.[17,18]. Finally, the small line at 560.8 nm in Fig. 4(c) is attributed to the negatively charge exciton X^- in[19]. We note a large splitting of 5.66 nm (22.4 meV) between the X and XX lines.

At room temperature, the zero-phonon lines are vanishingly small, and the spectra only shows broad phonon sidebands. The fits of the spectra of Fig. 2 at P =6 µW and of the inset of Fig. 3(a) are shown in Fig. 4(a) and (b) respectively. They comprise four Voigt functions and a constant baseline. The position of each line is set to match the relative po-

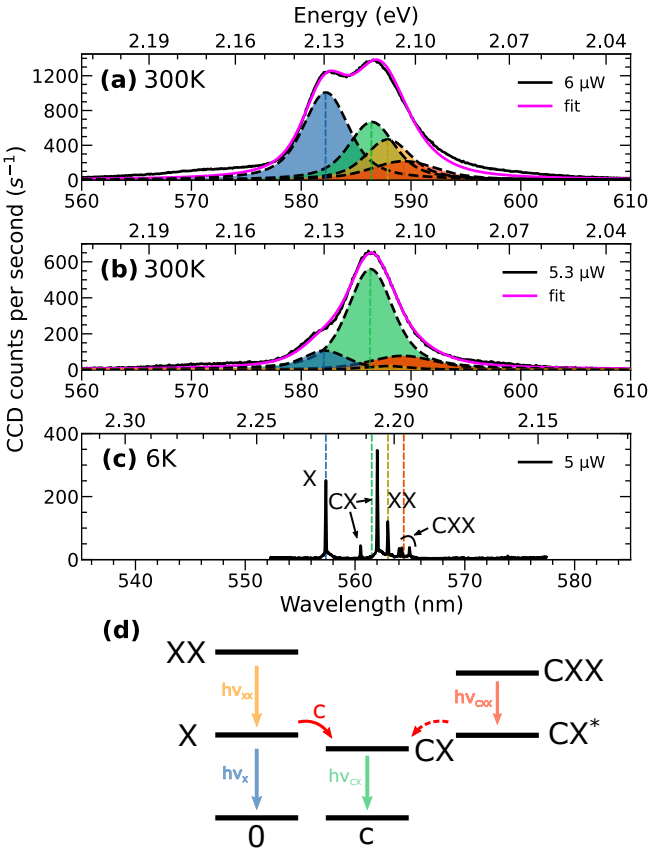

Figure 4: PL measurements on the same NW as in Fig. 1(b). **(a)** Spectrum under 6 µW excitation at room temperature. The signal is fitted (magenta curve) with a sum of four Voigt functions, resulting in the blue, green, yellow and red filled-lines. The same method is applied for the spectrum after intensity decrease in **(b)**. **(c)** Spectrum performed at 6K, under 5 µW pulsed excitation, with grating 1800 grooves/mm, slits 0.05 mm. The wavelength range was shifted to match the X lines with the 300K spectrum. In all the spectra, constant baselines have been removed (electronic noise). **(d)** Schematic diagram of different mechanisms possibly involved in the luminescence process: the simple radiative cascade (neutral or charged) and the cross-radiative cascade. In the last mechanism, the QD is repopulated with an extra charge, c, resulting in CX.

sitions of the X, CX, XX, and CXX lines in Fig. 4(c). The X, CX, and XX linewidths are constrained to a common value, while CXX, composed of several lines, has a larger width. Assuming that the trapping of electron-hole pairs does not depend on the presence of charges in the QD, the amplitude of each line is set so that the ratios of intensities obey $I_{XX}/I_X = I_{CXX}/I_{CX}$.

The fit in Fig. 4(b) results in a X, CX, and XX linewidth equal to 5.2 nm (19 meV), and 7.2 nm (26.4 meV) for CXX. The common biexciton/exciton intensity ratio is 0.45, illustrating that we are not fully at saturation at P =6 µW. Although X is dominant in Fig. 4 (a), the contribution of CX is relatively important with $I_{CX}/(I_{CX} + I_X) = 0.40$. The lines X and CX together yield 0.17 photon per pulse.

The ratios $I_{XX}/I_X = I_{CXX}/I_{CX} = 0.28$ in Fig. 4 (b) indicate that either the spectrum (after the intensity decrease) is further away from saturation, or that non-radiative processes reduce the X emission intensity. Additionally, the ratio $I_{CX}/(I_{CX} + I_X) = 0.82$ shows that CX dominates to a large extent X. In Fig. 4 (b), X and CX lines together contribute for 0.06 photon per pulse. Moreover, the fit in Fig. 4(b) shows that the strongest contribution at 585.0 nm is due to the CX line (blue arrow in Fig. 3(a) inset), with a small overlap with CXX and X lines. The corresponding decay curve (Fig 3(a)) exhibits a dominant exponential decay with a sub-nanosecond lifetime ($\tau_2 = 0.74$ ns), a value slightly larger than

the lifetime reported in Ref.[12]. Moreover, the small contribution from the rising exponential decay ($|A_1| \ll A_2$) signal is in good agreement with an excitation power far from saturation.

We also investigated the impact of the spectral window position on the emitter's purity. At 585.0 nm (blue arrow in the inset of Fig. 3(a), the zero-delay correlation peak is $g^2(0) = 0.3$. We measure $g^2(0) = 0.4$ close to L2 peak center (green arrow labeled as 2 in the inset) and $g^2(0) = 0.6$ on the red side of L2 (red arrow labeled as 3). See Supplement 1 for additional data. Shifting from spectral window 1 to 3, the overlap between CX and CXX increases, enhancing a correlation through the biexciton-exciton cascade in the charged QD. Coming back to spectral window 1, there is still some CX-CXX overlap at 585.0 nm but we cannot rule out the possibility of a cross radiative cascade resulting from a fast charge trapping forming the positively charged exciton $X + h \rightarrow X^+$, as illustrated in Fig. 4(d). We may expect to increase the purity even more ($g^2(0) < 0.3$) by blue-shifting the spectral window below 585 nm. This would make it possible to identify the role of the cross-cascade. However, the intensity diminishes drastically as we shift the spectral window to lower wavelength. There is an unavoidable tradeoff between purity which requires a narrow spectral window, and brightness, where a broad spectral bandwidth with high intensity is needed.

In conclusion, we demonstrated a promising on-demand SPS operational at room temperature, with large X-XX splitting of 5.66 nm (22.4 meV), enabling us to obtain a high single-photon purity with $g^2(0) < 0.3$. Combining X and CX lines, we demonstrate a SPS brightness ranging from 0.17 photon per pulse initially (i.e. an emission rate of 13 MHz with a 76 MHz excitation rate) to 0.06 after intensity decrease (i.e. 4.5 MHz)[4]. The observed subnanosecond decay time would allow a much higher repetition rate towards the GHz range. Further improvements are necessary to address the observed charging effect. Additional non-resonant laser excitation may be used to fill the traps surrounding the QD. Alternatively, modifying the growth conditions[19] and surface passivation of the NW may also effectively mitigate surface states from serving as traps for charge carriers. Lower temperatures down to to 220K (achieved using a Peltier cooler) can be used to reduce the linewidths and hence the overlap between lines undergoing a radiative cascade. Intermediate temperature measurements are under progress to better understand the phenomena and further optimize the SPS performances. The efficient coupling between the guided mode in the NW and free-space paves the way for integrating the SPS into a variety of photonic devices[20].

ACKNOWLEDGMENTS

The substrate has been patterned by lithography at the NanoFab cleanroom facility of Institut Néel, Grenoble. Thanks are due to Yann Genuist for his participation to the growth of samples.

FUNDING

We acknowledge funding from the Laboratoire dexcellence LANEF in Grenoble, ANR-10-LABX-51-01, and CEA-PE Bottom-Up QPhotonics.

DISCLOSURES

The authors declare no conflicts of interest.

DATA AVAILABILITY STATEMENT

Data may be obtained from the authors upon reasonable request.

SUPPLEMENTAL DOCUMENT

See Supplement 1 for supporting content.

REFERENCES

[1] Yasuhiko Arakawa and Mark J. Holmes. Progress in quantum-dot single photon sources for quantum information technologies: A broad spectrum overview. *Applied Physics Reviews*, 7(2):021309, June 2020. Publisher: American Institute of Physics.

[2] N. Somaschi, V. Giesz, L. De Santis, J. C. Loredo, M. P. Almeida, G. Hornecker, S. L. Portalupi, T. Grange, C. Antón, J. Demory, C. Gómez, I. Sagnes, N. D. Lanzillotti-Kimura, A. Lemaítre, A. Auffeves, A. G. White, L. Lanco, and P. Senellart. Near-optimal single-photon sources in the solid state. *Nature Photonics*, 10(5):340–345, May 2016. Number: 5 Publisher: Nature Publishing Group.

[3] Julien Claudon, Joël Bleuse, Nitin Singh Malik, Maela Bazin, Périne Jaffrennou, Niels Gregersen, Christophe Sauvan, Philippe Lalanne, and Jean-Michel Gérard. A highly efficient single-photon source based on a quantum dot in a photonic nanowire. *Nature Photonics*, 4(3):174–177, March 2010. Number: 3 Publisher: Nature Publishing Group.

[4] Yu Zhou, Ziyu Wang, Abdullah Rasmita, Sejeong Kim, Amanuel Berhane, Zoltán Bodrog, Giorgio Adamo, Adam Gali, Igor Aharonovich, and Wei-bo Gao. Room temperature solid-state quantum emitters in the telecom range. *Science Advances*, 4(3):eaar3580, March 2018.

[5] Saniya Deshpande, Thomas Frost, Arnab Hazari, and Pallab Bhattacharya. Electrically pumped single-photon emission at room temperature from a single ingan/gan quantum dot. *Applied Physics Letters*, 105(14):141109, 2014.

[6] Ling Chen, Bowen Sheng, Shanshan Sheng, Ping Wang, Xiaoxiao Sun, Duo Li, Tao Wang, Renchun Tao, Shangfeng Liu, Zhaoying Chen, Weikun Ge, Bo Shen, and Xinqiang Wang. Room temperature triggered single photon emission from self-assembled gan/aln quantum dot in nanowire. *Advanced Functional Materials*, 32(47):2208340, 2022.

[7] S. Bounouar, M. Elouneg-Jamroz, M. den Hertog, C. Morchutt, E. Bellet-Amalric, R. André, C. Bougerol, Y. Genuist, J.-Ph. Poizat, S. Tatarenko, and K. Kheng. Ultrafast Room Temperature Single-Photon Source from Nanowire-Quantum Dots. *Nano Letters*, 12(6):2977–2981, June 2012. Publisher: American Chemical Society.

[8] Dong-Dong Li, Qi Shen, Wei Chen, Yang Li, Xuan Han, Kui-Xing Yang, Yu Xu, Jin Lin, Chao-Ze Wang, Hai-Lin Yong, Wei-Yue Liu, Yuan Cao, Juan Yin, Sheng-Kai Liao, and Ji-Gang Ren. Proof-of-principle demonstration of quantum key distribution with sea-water channel: towards space-to-underwater quantum communication. *Optics Communications*, 452:220–226, 2019.

[9] Niels Gregersen, Torben R. Nielsen, Julien Claudon, Jean-Michel Gérard, and Jesper Mørk. Controlling the emission profile of a nanowire with a conical taper. *Optics Letters*, 33(15):1693–1695, August 2008. Publisher: Optica Publishing Group.

[10] Ali Jaffal, Walid Redjem, Philippe Regreny, Hai SonăNguyen, Sébastien Cueff, Xavier Letartre, Gilles Patriarche, Emmanuel Rousseau, Guillaume Cassabois, Michel Gendry, and Nicolas Chauvin. InAs quantum dot in a needlelike tapered InP nanowire: a telecom band single photon source monolithically grown on silicon. *Nanoscale*, 11(45):21847–21855, 2019. Publisher: Royal Society of Chemistry.

[11] Saransh Raj Gosain, Edith Bellet-Amalric, Martien den Hertog, Régis André, and Joël Cibert. The onset of tapering in the early stage of growth of a nanowire. *Nanotechnology*, 33(25):255601, April 2022. Publisher: IOP Publishing.

[12] Saransh Raj Gosain. *Room temperature single-photon source based on semiconductor quantum-dot nanowire for integrated photonics*. phdthesis, Université Grenoble Alpes [2020-....], December 2021.

[13] Gabriele Bulgarini, Michael E. Reimer, Maaike Bouwes Bavinck, Klaus D. Jöns, Dan Dalacu, Philip J. Poole, Erik P. A. M. Bakkers, and Val Zwiller. Nanowire Waveguides Launching Single Photons in a Gaussian Mode for Ideal Fiber Coupling. *Nano Letters*, 14(7):4102–4106, July 2014. Publisher: American Chemical Society.

[14] Mitutoyo corporation, 20-1, Sakado 1-Chome, Takatsu-ku, Kawasaki-shi, Kanagawa 213-8533, Japan. *Microscope units and objectives (UV, NUV, VISIBLE & NIR region)*.

[15] TCSPC Performance of the id100-50 detector, Becker and Hickl GmbH (2005), https://www.photonicsolutions.co.uk/upfiles/id100-50-becker.pdf.

[16] Saransh Raj Gosain, Edith Bellet-Amalric, Eric Robin, Martien Den Hertog, Gilles Nogues, Joël Cibert, Kuntheak Kheng, and David Ferrand. Quantitative analysis of the blue-green single-photon emission from a quantum dot in a thick tapered nanowire. *Physical Review B*, 106(23):235301, December 2022. Publisher: American Physical Society.

[17] Samir Bounouar. *Photon correlations on a room temperature semi-conductor single photon emitter*. phdthesis, Université de Grenoble, February 2012.

[18] I. A. Akimov, A. Hundt, T. Flissikowski, and F. Henneberger. Fine structure of the trion triplet state in a single self-assembled semiconductor quantum dot. *Applied Physics Letters*, 81(25):4730–4732, December 2002. Publisher: American Institute of Physics.

[19] Mathieu Jeannin, Thibault Cremel, Teppo Häyrynen, Niels Gregersen, Edith Bellet-Amalric, Gilles Nogues, and Kuntheak Kheng. Enhanced Photon Extraction from a Nanowire Quantum Dot Using a Bottom-Up Photonic Shell. *Physical Review Applied*, 8(5):054022, November 2017. Publisher: American Physical Society.

[20] Khaled Mnaymneh, Dan Dalacu, Joseph McKee, Jean Lapointe, Sofiane Haffouz, John F. Weber, David B. Northeast, Philip J. Poole, Geof C. Aers, and Robin L. Williams. On-Chip Integration of Single Photon Sources via Evanescent Coupling of Tapered Nanowires to SiN Waveguides. *Advanced Quantum Technologies*, 3(2):1900021, 2020. reprint: https://onlinelibrary.wiley.com/doi/pdf/10.1002/qute.201900021.

Brightness and purity of a room-temperature single-photon source in the blue-green range: supplemental document

1. CALIBRATION OF THE EXPERIMENTAL SETUP

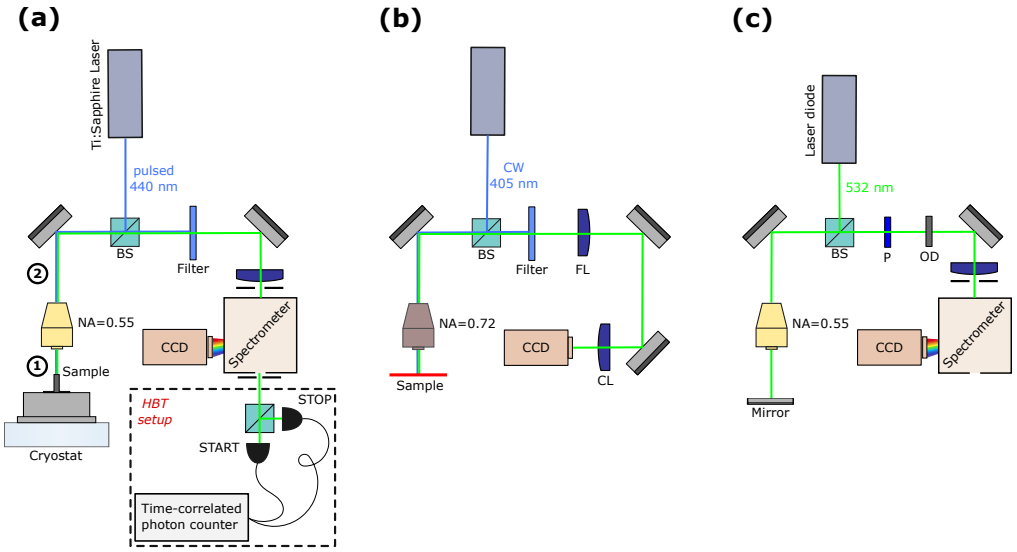

Fig. S1. Schematics of the spectroscopy setups. **(a)** TRPL setup. BS: beam-splitter; **(b)** Setup used for Fourier imaging technique. FL: Fourier Lens; CL: Collection Lens. **(c)** Schematic of the setup calibration. OD: Optical Density; P: Polarizer

A. Experimental setup

The setup used for micro-PL and TRPL measurements presented in the article (at 6K and 300K) is displayed in Figure S1 (a). The sample was positioned on a continuous flow cold-finger cryostat, which can cool the sample down to 5-6 K for cryogenic measurements. The cryostat is mounted on a X-Y linear stage, enabling high precision and smooth motion control. The excitation is provided by a frequency doubled pulsed Ti:Sapphire laser at 440 nm. This results in pulses (< 2 ps) with a repetition frequency of $f_{\text{rep}} = 76$ MHz that excite the NW along its axis. A $NA = 0.55$ M Plan apo SL 100X Mitutoyo microscope objective is used to focus the excitation laser on a selected NW-QD and to collect the QD emittted light. Emission spectra are recorded using a Horiba Jobin Yvon HR-460 spectrometer and a DU920P-BEX2-DD Andor CCD camera. Second-order correlation measurements are performed on an HBT setup equipped with two ID Quantique single-photon detectors (ID100-50) mounted on the side exit of the spectrometer. The correlations are computed using a SPC-130 Becker and Hickl time-correlated photon counting module (TCSPC).

For the Fourier imaging technique, a second setup (Figure S1 (b)) is used, which extends the confocal microscopy setup with an additional lens (Fourier lens in Figure S1 (b)). The lens is used to project the back focal plane of the objective (image plane) onto a CCD camera, enabling Fourier imaging of the emitter.

B. Setup calibration and emission line brightness

In this paper, we define the brightness of an emission line (B_{line}) as the average photon number transmitted by the microscope objective for each laser excitation pulse (*i.e* the averaged photon number per pulse measured at the position 2 of Figure S1.a). Note that the brightness is sometimes defined in the literature as the photon number collected by the microscope objective (*i.e* the averaged photon number per pulse measured at the position 1 of Figure S1.a). At the QD emission wavelength, about 10% of QD emission is lost in the microscope objective and B_{line} represents an effective brightness that can be used for practical implementations. For a pulsed laser excitation with the repetition frequency f_{rep}, B_{line} is directly related to the line emission rate γ_{line} measured at the position 2:

$$B_{\text{line}} = \frac{\gamma_{\text{line}}}{f_{\text{rep}}} \tag{S1}$$

For the measurements done with the set-up shown in Figure S1.(a), we compute the line emission rate γ_{line} from the integrated count rate (γ_{CCD}) of the CCD spectra recorded under pulsed excitation : $\gamma_{\text{line}} = \epsilon\gamma_{\text{CCD}}$ where ϵ is the set-up collection efficiency.

To evaluate ϵ at the QD emission wavelength (580 to 590 nm), we use an attenuated 532 nm cw laser diode (see Figure S1.c). The value of ϵ was deduced from the ratio of the laser diode integrated CCD spectra and the laser power measured in front the optical density (OD=4). At this particular wavelength, we observe that ϵ does not depend on the the incident polarization. The influence of the spectrometer entrance slit and of the spot size was carefully taken into account. The transmission of the 50/50 injection beam splitter was also controlled at the laser diode wavelength. Please note that the CCD camera was used with an internal gain of 10 (one CCD count corresponding to 10 detected photons).

2. ADDITIONAL DATA

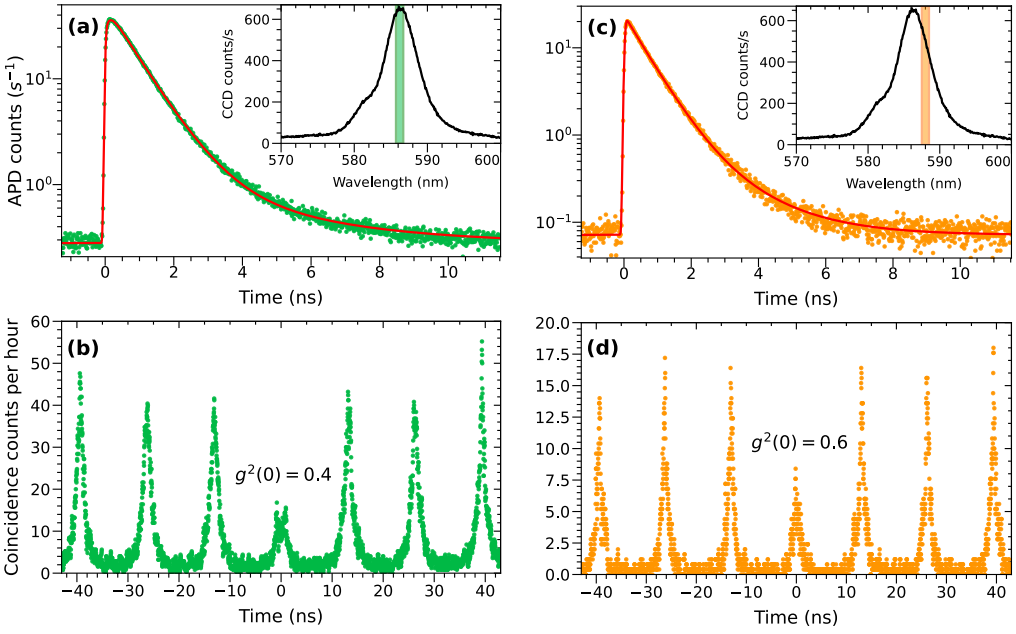

Fig. S2. Room temperature TRPL measurements on the NW studied through the article. **(a)** Decay time of the QD-NW under 5 µW excitation power at 586.2 ± 0.5 nm (green symbols) and 588.0 ± 0.5 nm in **(c)** (orange symbols). An exponential decay model is used to fit the signals (red curves). **(b)** Second-order intensity correlation function at 4.8 µW. The data are averaged over seven channels. The traces exhibit $g^2(0) = 0.4$ at 586.2 nm (green symbols), and in **(d)** $g^2(0) = 0.6$ at 588.0 nm (orange symbols).

Additional TRPL data are presented in Figure S2, for two spectral window positions (centered at 586.2 nm and 588 nm). Table S1 shows the parameters used to fit the decay time curves shown in Figure S2 (a) and (c) insets.

Table S1. Values of parameters used in Figure S2 (a) and (c)

Window central position (nm)	Contribution	A_i	τ_i (ns)
586.2	Rise (i = 1)	-2.76	0.12
	Fast decay (i = 2)	39.85	0.81
	Slow decay (i = 3)	4.16	3.07
588.0	Rise (i = 1)	0	
	Fast decay (i = 2)	13.93	0.64
	Slow decay (i = 3)	2.41	1.65